System identification of a soft manipulator with polynomial methods

Tiago Barretto Sant'Anna, Pedro Machado, Emanuel Benício, Lucas Silva
Robotics Department
Senai CIMATEC, Salvador, Brazil
tiagobarreto581@gmail.com, pedrosantosm@outlook.com, emanuel.cajueiro@fieb.org.br, lucas.cs@fieb.org.br

***Abstract*—This paper explores system identification techniques within the domain of soft robotics, focusing specifically on a tendon-actuated soft manipulator. The primary goal is to perform system identification for this manipulator using two distinct mathematical models: ARX (Auto-Regressive with eXogenous input) and ARMAX (Auto-Regressive Moving Average with eXogenous input). The manipulator system is driven by three motors, and the piecewise constant curvature parameters, θ and ϕ, are considered as outputs. The comparative analysis reveals that the effectiveness of these identification methods varies according to system dynamics. The ARX model performs well with simpler dynamics like those of ϕ, while the ARMAX model proves superior for more complex or noisy systems like θ, owing to its inclusion of moving average components that capture additional dynamics. These findings underscore the importance of selecting the appropriate model based on specific system characteristics for accurate modeling and prediction.**

***Index Terms*—Soft robots; system identification; polynomial methods; multivariable systems; soft manipulator.**

I. Introduction

Soft robotics has emerged as a promising field by utilizing flexible and adaptable materials to design robotic systems capable of interacting safely and effectively with dynamic environments and humans. However, the inherent complexity of soft systems poses significant challenges in identifying and modeling their behavior, which is crucial for the effective design and control of these robots. According to (8), developing a mathematical model that accurately describes deformation configurations is a significant obstacle in this field. In this context, system identification provides essential insights into the dynamic and static characteristics of soft systems.

Various approaches, ranging from detailed physical models to data-based methods and machine learning techniques, were employed to study the existing research and construct the methodology for this investigation. (9) offers an alternative model for the dynamics of multi-session soft manipulators using a discrete Cosserat approach. Additionally, (1) discusses a data-driven method to identify models of soft manipulators, enabling consistent control under varying load conditions.

(10) compares two methods using a data-based model relying solely on mechanical feedback for stable control of the flexible robotic manipulator. Another notable contribution is made by (2), which presents a closed-loop controller based on a neural network trained with a deep reinforcement learning algorithm known as Trust Region Policy Optimization.

The primary objective of this work is to identify a mathematical model that can infer the position of a soft manipulator's tip based on motor actuation. To achieve this, two polynomial system identification algorithms—ARX and ARMAX—were employed. Additionally, this work aims to analyze the optimal function identified and gain insights into its behavior.

II. Background Study

A. Soft Manipulator

Unlike conventional robots with predictable movements, soft robots can deform in complex ways, complicating their control (12). Developers use advanced strategies, including adaptive control systems and machine learning, to manage their infinite degrees of freedom and non-linear behavior (11).

Phenomenological models of soft robots use physical and mathematical models to represent systems. This approach establishes relationships between inputs, such as actuator movement, and outputs like movements or deformations (13). While phenomenological methods streamline prediction and control of soft robotics, they often leave gaps in representation of complex dynamics. Empirical models simplify model creation, particularly when the physics are not well understood. When frequently updated, these models can estimate parametric variations.

System identification techniques such as AutoRegressive with eXogenous inputs (ARX) and AutoRegressive Moving Average with eXogenous inputs (ARMAX) are examples of empirical models. These models use input-output data to predict dynamic systems behavior, aiding in the creation of control strategies that adjust to real-time feedback and environmental changes, thereby enhancing soft robots functionality and adaptability.

B. ARMAX

The ARMAX model enhances the ARMA framework by integrating exogenous variables into time series analysis and forecasting (7). It combines autoregressive terms with moving averages and external factors, capturing both historical dependencies and the impact of external variables for improved prediction accuracy and insight (4).

The mathematical structure of the ARMAX model is captured in the following equations (6):

$$A(q)y(t) = B(q)u(t - n_b) + C(q)e(t) \quad (1)$$

Where equation (1) defines the relationship between the output $y(t)$, the controllable input $u(t - n_b)$ with a delay n_b, and the error term $e(t)$. The polynomials $A(q)$, $B(q)$, and $C(q)$ are defined as:

$$A(q) = 1 + a_1 q^{-1} + \cdots + a_{n_a} q^{-n_a} \quad (2)$$
$$B(q) = b_1 + b_2 q^{-1} + \cdots + b_{n_b} q^{-n_b+1} \quad (3)$$
$$C(q) = 1 + c_1 q^{-1} + \cdots + c_{n_c} q^{-n_c} \quad (4)$$

Here, the coefficients a_i, b_i, and c_i are model parameters that are estimated from time series data. The operator q^{-1} represents a one-time unit delay, introducing a temporal dimension in the modeling of dynamic relationships.

III. Methodology

Data collection was performed using ArUco (3) markers. This data was then represented in the format of piecewise constant curvature (PCC) (5). Finally, the data was filtered, a study of the correlation between inputs and outputs was conducted, and system identification was performed.

A. ArUco Dataset

For the development of this work the authors collected three data sets. The dataset was compiled by recording the position coordinates and orientation of the flexible manipulator in its dynamic behavior, which was fed with the tendon lengths produced by a signal of Amplitude Modulated Pseudo-Random Bit Sequences (APRBS). This data was colected with a frequency of 25 Hz.

The ArUco tags provide position and orientation data for each spring in the manipulator structure, captured by a mono camera. Data were collected regarding three flexible manipulators, which have, respectively, 1, 3, and 5 springs. These devices feature a single session of operation and three motors responsible for regulating the length of three tendons. Figure 1 displays the application of ArUco tags on the five mentioned manipulators.

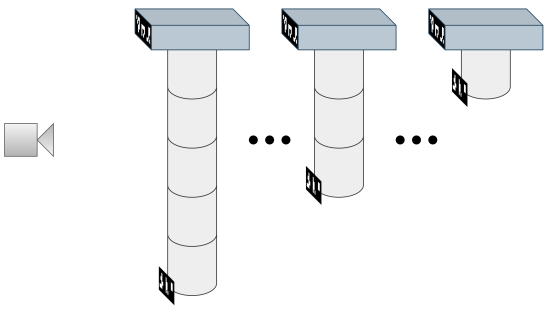

Fig. 1: Configurations of the manipulator with flexible structures, containing 5, 3 and 1 springs.

The data contained in the dataset cover the length of the three cables (expressed in meters), as well as the position (x, y, z) and orientation (quaternion, roll, pitch, yaw) information of both the base and each spring present in the manipulator. For the manipulator containing one spring, the dataset consists of 4049 samples. The dataset for the manipulator with three springs contains 3603 samples; and for the manipulator with five springs, the dataset is comprised of 3227 samples.

B. Piecewise Constant Curvature Model

After collecting data in spatial coordinates (x, y, z), they were converted into the Piecewise Constant Curvature (PCC) representation (5). A schematic of this model is represented in Figure 2. Each segment is then modeled as a curve with constant curvature described by two parameters: θ and ϕ. θ represents the bending curvature of the segment, analogous to the angle of curvature in classical geometry. ϕ captures the twisting curvature, reflecting the amount of rotation along the segment's longitudinal axis. This approach simplifies the model by reducing the manipulator's infinite degrees of freedom to a finite set of curvature pairs (θ_i, ϕ_i) for each segment i.

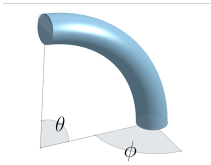

Fig. 2: Constant curvature diagram

C. Filter design

The development of systems identification required the implementation of a finite impulse response (FIR) low-pass filter to reduce noise of the obtained data. The FIR filter was selected for its ability to maintain the linear phase of signals, for preserving the temporal integrity of the original data. By setting the cutoff at 0.2 Hz, as showed in Figure 3, the filter attenuates higher frequencies, including noise while preserving important lower frequency components below 0.2 Hz.

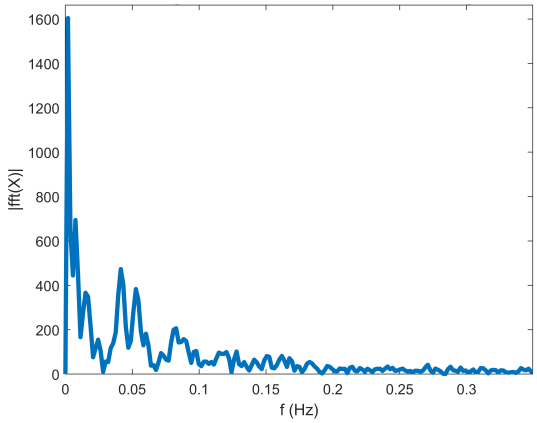

Fig. 3: Fast fourrier transform spectrum of the singnal with a spring

This filter was applied to all the datasets collected to support the training and validation of the system identification process.

D. Correlation analysis

The correlation results for robotic manipulators with one, three, and five springs are presented in Figure 4. These correlations were computed using the Pearson correlation coefficient, defined as:

$$r_{xy} = \frac{\sum_{i=1}^{n}(x_i - \bar{x})(y_i - \bar{y})}{\sqrt{\sum_{i=1}^{n}(x_i - \bar{x})^2} \cdot \sqrt{\sum_{i=1}^{n}(y_i - \bar{y})^2}}, \quad (5)$$

where x_i and y_i are the input (cable tension) and output (angle φ or θ signals, respectively, and n is the number of data points.

To provide a comprehensive assessment of the temporal relationship between input tensions and output angles, the correlation functions were computed over a wide lag window, extending up to 20,000 samples in some cases. This range was selected to ensure that both immediate and delayed dependencies could be fully observed, especially given the differing dynamic responses of each manipulator configuration. The differences in the x-axes (lag values) among Figures 4a, 4b, and 4c reflect the unique physical properties and time constants of each manipulator. For example, manipulators with more springs and greater structural complexity tend to exhibit longer response times, requiring a broader lag window to capture the full extent of their input-output correlations. Consequently, the lag range for each plot was tailored to the specific system to accurately represent its dynamic behavior and avoid truncation of relevant correlation information.

In the case of the one-spring manipulator (Figure 4a), the correlation curves between cable tensions and the output angles exhibit a nearly symmetric triangular pattern around the central lag. This indicates a strong and temporally aligned linear relationship between the actuation and the resulting motion.

For the three-spring configuration (Figure 4b), the correlation curves from different cables begin to overlap, and the triangular shape becomes sharper and more centralized. This suggests a higher degree of predictability and a stronger linear dependence between inputs and outputs, reinforcing the deterministic nature of the system's behavior.

In contrast, the five-spring manipulator (Figure 4c) exhibits more complex correlation profiles. While the curves still show a clear linear trend around the zero-lag region, the intertwining among the signals becomes more pronounced. This is likely due to the increased structural complexity—comprising multiple springs connected by rigid elements—which introduces additional dynamic interactions. Nevertheless, the persistence of high correlation near zero lag confirms that the system retains a predominantly linear character.

Overall, the results suggest that as the number of springs increases, the correlations between cable tensions and angular displacements become more complex, but the underlying linear relationship remains evident. This is characteristic of systems with multiple degrees of freedom, where the actuation of individual cables produces interdependent effects due to mechanical coupling.

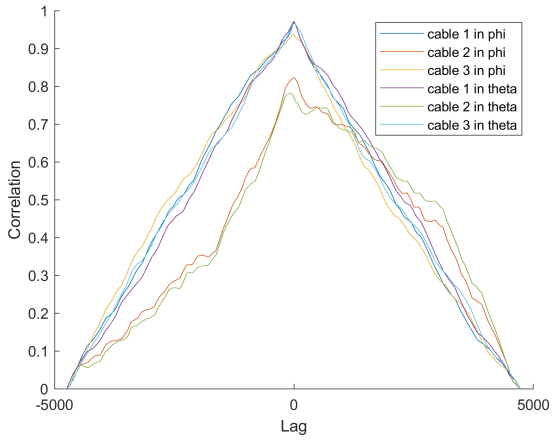

(a) one-spring manipulator

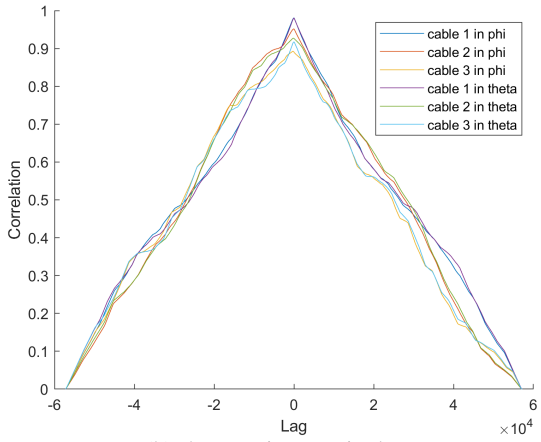

(b) three-spring manipulator

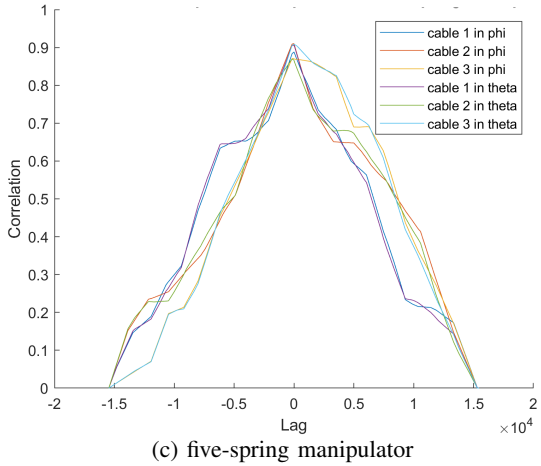

(c) five-spring manipulator

Fig. 4: Correlation for manipulators.

E. System identification

To work with system identification, the curvature model generated two models: one focused on predicting θ, and another aimed at solving ϕ. In both systems, the input is the rotation of the motors that operate the manipulator

To carry out system identification, MATLAB software was

used. Its libraries for system identification and filter design were utilized. To find the best parameters for the ARX and ARMAX models, loop structures were used to test all possible combinations from first to tenth order in each parameter. The model with the best fit was then selected.

The computer chosen for this development had the following specifications: Windows 10 operating system, 12th Gen Intel(R) Core(TM) i5-12450H processor, and 8GB RAM.

IV. Results

The comparative analysis of system identification techniques for single-spring systems labeled ϕ and θ in 5 reveals distinctive modeling dynamics. The ϕ system showed in 5b demonstrates minimal variance between the ARX and ARMAX methodologies, with the fits being 58.38% and 58.74%, respectively. This negligible difference suggests that the inclusion of the moving average process in the ARMAX model does not significantly benefit the ϕ system's identification.

In this work, the term "fit" refers to the quantitative measure used to evaluate how accurately the identified models reproduce the system's output. The fit percentage is calculated as follows:

$$\text{Fit } (\%) = 100 \times \left(1 - \frac{\|y - \hat{y}\|}{\|y - \bar{y}\|}\right) \tag{6}$$

where y represents the measured output, $\hat{y}$ is the output predicted by the model, and $\bar{y}$ is the mean of the measured output. A fit of 100% indicates perfect agreement between the model and the measured data, while lower values represent increasing deviation. This metric provides a standardized way to compare model performance across different identification algorithms and system configurations.

In contrast, the θ system's, visualized in Figure 5a, results are strikingly different, with the ARX model attaining a 59.8% fit while the ARMAX model exhibits a superior fit of 71.72%. This increment highlights the ARMAX model's enhanced capability in capturing the underlying processes of the θ system, suggesting that the moving average parameters are instrumental in accounting for the noise or unmodeled dynamics present within this particular system.

These outcomes emphasize the importance of model selection in system identification. While the ARX model suffices for the ϕ system, the θ system benefits from the additional complexity provided by the ARMAX model, underscoring the need for a tailored approach based on the specific characteristics and responses of the system in question.

The system identification processes for the Figure 6 ϕ and θ systems, each incorporating a trio of springs, present intriguing contrasts in model fidelity. In the case of the image 6b ϕ system, the ARMAX model, imbued with both autoregressive and moving average elements, showcases a markedly superior fit of 83.94% compared to the simpler ARX model's 73.01%. This pronounced disparity underscores the ARMAX model's enhanced capability to embody the more complex dynamics inherent in the ϕ system.

The θ system's, seen in 6a, modeling outcomes narrate a different story. Here, the ARX model's fit stands at 84.29%,

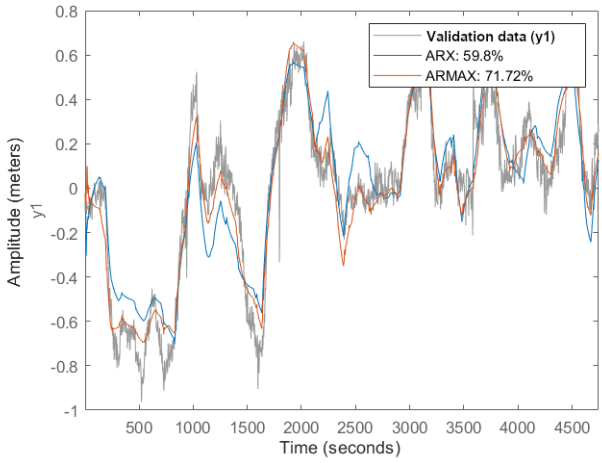

(a) Comparison of simulated response with θ with one spring

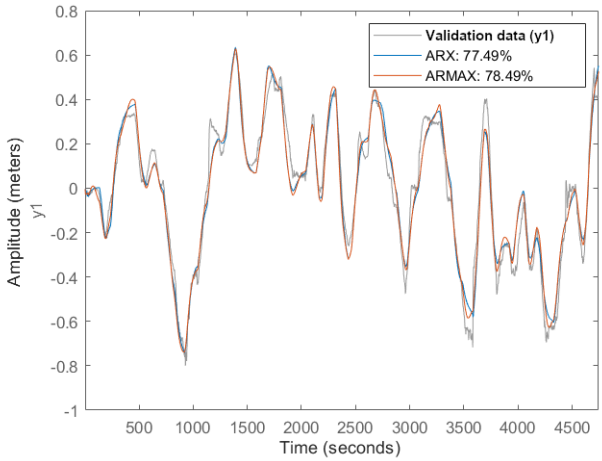

(b) Comparison of simulated response with ϕ with one spring

Fig. 5: Comparison of simulated response for one spring

with the ARMAX model offering a marginally improved fit of 84.89%. This subtle difference intimates that for the θ system, the additional complexity introduced by the ARMAX model may not be as critical to capturing the system's behavior.

These insights accentuate the nuanced nature of system identification. They bring to light that the optimal choice between ARX and ARMAX models is not merely a function of model sophistication but is closely tied to the unique dynamics of each system. While the ϕ system evidently benefits from the ARMAX model's structure, the θ system does not exhibit a significant preference, suggesting that simpler models could suffice in certain contexts.

The dynamics of the ϕ and θ systems in Figure 7, each integrating five springs, have been meticulously modeled using ARX and ARMAX identification methods. For the Figure 7b (ϕ) system, the analysis revealed that the ARMAX model achieved a marginally superior fit of 78.65% compared to the ARX model's 76.39%. This indicates a modest enhancement in capturing the system's response, hinting at the potential benefits of the moving average component inherent in the

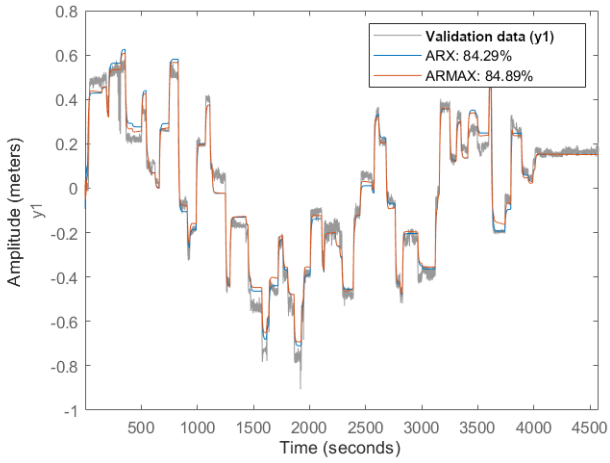

(a) Comparison of simulated response with θ with three springs

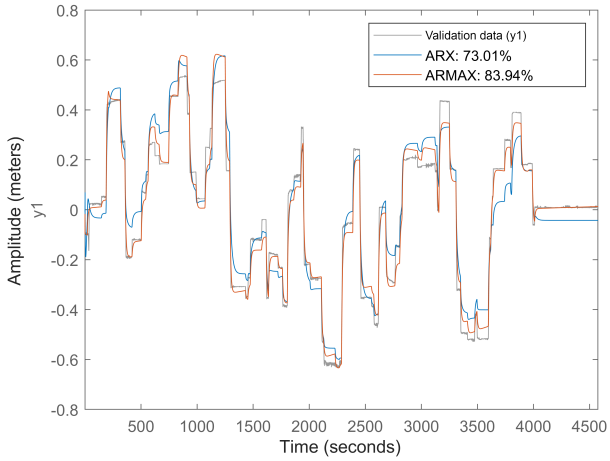

(b) Comparison of simulated response with ϕ with three springs

Fig. 6: Comparison of simulated response for three springs

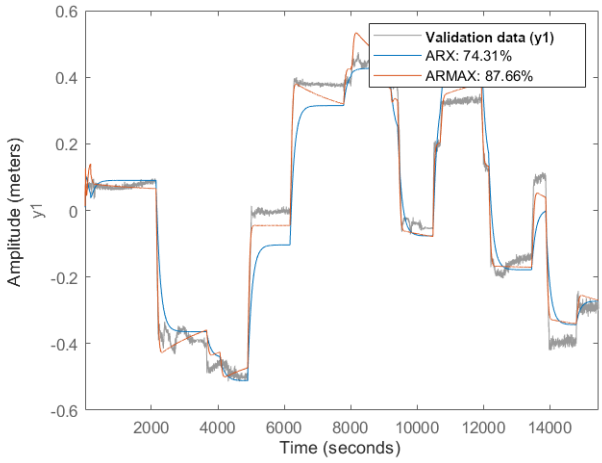

(a) Comparison of simulated response with θ with five springs

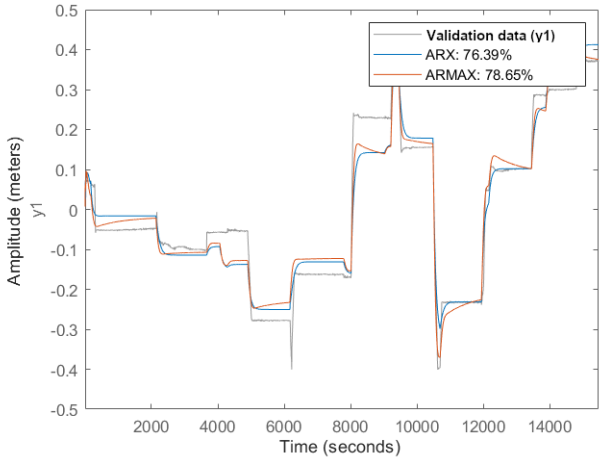

(b) Comparison of simulated response with ϕ with five springs

Fig. 7: Comparison of simulated response for five springs

ARMAX model.

The modeling of the θ system uncovered a pronounced divergence between the two methods, that can be seen in Figure 7a, with the ARMAX model significantly eclipsing the ARX model by exhibiting a fit of 87.66%, in contrast to 74.31%. Such a distinct improvement accentuates the ARMAX model's robustness in assimilating the system's behavior, possibly due to its more sophisticated structure which encompasses both autoregressive and moving average mechanisms.

These insights underline the pivotal role of model selection in the realm of system identification. They demonstrate that while the ARX model offers a commendable baseline for system approximation, the ARMAX model emerges as a more potent tool, especially in scenarios where the system dynamics are considerably complex.

A. System analisys

For the study of the system, the model featuring a three-spring configuration was chosen to analyze the ϕ parameter. This particular setup of the three-spring manipulator was selected due to its superior response in predictive models. The ϕ curvature parameter was specifically chosen due to its complex relationship with various input cables.

The parameters of the ARMAX algorithm can be observed in the following equations:

$$A(q) = 1 - 2.186q^{-1} + 1.515q^{-2} - 0.8448q^{-3} + 0.808q^{-4} - 0.3525q^{-5} + 0.2083q^{-6} - 0.1479q^{-7} \tag{7}$$

$$B_1(q) = 0.0002074q^{-2} + 0.001366q^{-3} + 0.0006506q^{-4} - 0.003117q^{-5} + 0.00162q^{-6} - 0.003595q^{-7} + 0.002868q^{-8} \tag{8}$$

$$B_2(q) = 0.0005451q^{-2} - 0.0001531q^{-3} - 0.0005126q^{-4} - 0.0002479q^{-5} + 0.0008735q^{-6} - 0.001058q^{-7} + 0.0005526q^{-8} \tag{9}$$

$$B_3(q) = -0.0002921q^{-2} - 0.001571q^{-3} + 0.0004879q^{-4} + 0.0006211q^{-5} + 0.002573q^{-6} - 0.00058q^{-7} - 0.001239q^{-8} \tag{10}$$

$$C(q) = 1 - q^{-1} \tag{11}$$

In the ARMAX model framework for systems with multiple inputs, the parameters are outlined by a series of polynomial equations. The autoregressive component is represented by $A(q)$ (Equation 7), which indicates how past outputs influence current outputs. Each input's effect on the system is modeled by the polynomials $B_1(q)$, $B_2(q)$, and $B_3(q)$ (Equations 8, 9, and 10), detailing the specific influences of the three different input motors. The moving average component, $C(q)$ (Equation 11), captures the noise or random shocks affecting the system's output. These equations collectively provide a structure for analyzing and predicting the system behavior under the influence of multiple inputs.

The pole-zero map delineated in Figure 8 portrays the dynamic properties of the ϕ system, equipped with three springs. Each panel corresponds to distinct input channels (u1, u2, and u3), for each cable input, and showcases the system's poles and zeros—a reflection of its vibrational characteristics and stability.

As depicted in Figure 8, the left half-plane concentration of poles for inputs u1 and u3 signifies a stable system response, with the natural decay of vibrations assured by their negative real parts. In contrast, the poles and zeros associated with input u2 are confined within the unit circle in the complex plane, indicating a discrete-time stability criterion and potential resonant behavior. The layout of zeros, particularly for input u3, suggests distinct influences on the system's transfer function, emphasizing the importance of pole-zero placement in control system design and precision response tuning.

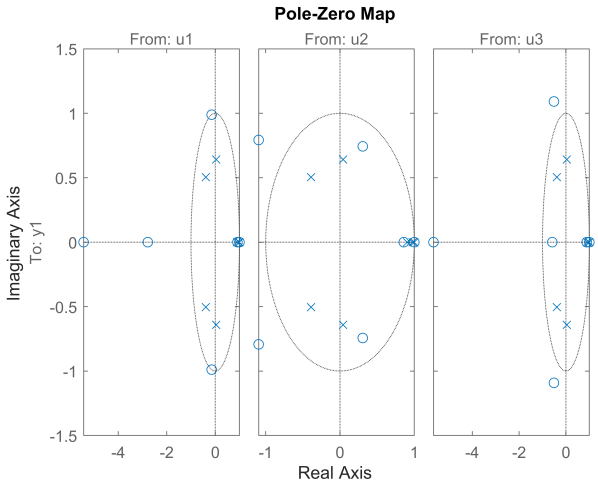

Fig. 8: Pole-zero map for the ϕ system with three springs.

V. Conclusion

This work presents techniques of system identification in the context of soft robots. The main objective was to produce a system identification of a soft manipulator actuate by tendons. For this development it was used two algorithms of system identification, ARX and ARMAX, to compare the results. And the system to identify it was a soft manipulator with three motors as inputs, and the piecewise constant curvature constants, θ and ϕ as output.

The analysis demonstrates that the effectiveness of ARX and ARMAX system identification methods varies significantly depending on the system dynamics. In systems like ϕ, where the dynamics are less complex, the ARX model generally provides adequate results. However, in more complex or noisy systems like θ, the ARMAX model proves more effective due to its ability to incorporate moving average components and capture additional dynamics. This emphasizes the necessity of selecting the appropriate model based on the specific characteristics of each system to ensure accurate modeling and prediction.

VI. Acknowledgments

The authors would like to acknowledge Shell Brasil Petróleo LTDA, the Brazilian Company for Industrial Research and Innovation (EMBRAPII), and Brazilian National Agency for Petroleum, Natural Gas and Biofuels (ANP) for the support and investments in RD&I.

References

[1] Daniel Bruder, Xun Fu, R Brent Gillespie, C David Remy, and Ram Vasudevan. Koopman-based control of a soft continuum manipulator under variable loading conditions. *IEEE Robotics and Automation Letters*, 6(4):6852–6859, 2021.

[2] Andrea Centurelli, Luca Arleo, Alessandro Rizzo, Silvia Tolu, Cecilia Laschi, and Egidio Falotico. Closed-loop dynamic control of a soft manipulator using deep reinforcement learning. *IEEE Robotics and Automation Letters*, 7(2):4741–4748, 2022.

[3] S. Garrido-Jurado, R. Muñoz-Salinas, F.J. Madrid-Cuevas, and M.J. Marín-Jiménez. Automatic generation and detection of highly reliable fiducial markers under occlusion. *Pattern Recognition*, 47(6):2280–2292, June 2014.

[4] Zheng Hui, Qin Lin-lin, and Wu Gang. Modeling and simulation of greenhouse temperature hybrid system based on armax model. In *2017 36th Chinese Control Conference (CCC)*. IEEE, July 2017.

[5] Mahboubeh Keyvanara, Arman Goshtasbi, and Irene A. Kuling. A geometric approach towards inverse kinematics of soft extensible pneumatic actuators intended for trajectory tracking, 2022.

[6] Lennart Ljung. *System identification*. Prentice Hall information and system sciences series. Prentice Hall, Philadelphia, PA, 2 edition, December 1998.

[7] Miaomiao Niu and Guohao Li. The impact of climate change risks on residential consumption in china: Evidence from armax modeling and granger causality analysis. *International Journal of Environmental Research and Public Health*, 19(19):12088, September 2022.

[8] Federico Renda, Costanza Armanini, Vincent Lebastard, Fabien Candelier, and Frederic Boyer. A geometric

variable-strain approach for static modeling of soft manipulators with tendon and fluidic actuation. *IEEE Robotics and Automation Letters*, 5(3):4006–4013, 2020.

[9] Federico Renda, Frédéric Boyer, Jorge Dias, and Lakmal Seneviratne. Discrete cosserat approach for multisection soft manipulator dynamics. *IEEE Transactions on Robotics*, 34(6):1518–1533, 2018.

[10] Thomas George Thuruthel, Egidio Falotico, Mariangela Manti, and Cecilia Laschi. Stable open loop control of soft robotic manipulators. *IEEE Robotics and Automation Letters*, 3(2):1292–1298, 2018.

[11] Lasitha Weerakoon, Zepeng Ye, Rahul Subramonian Bama, Elisabeth Smela, Miao Yu, and Nikhil Chopra. Adaptive tracking control of soft robots using integrated sensing skins and recurrent neural networks. In *2021 IEEE International Conference on Robotics and Automation (ICRA)*. IEEE, May 2021.

[12] Xuesong Yang, Linfeng Lan, Xiuhong Pan, Qi Di, Xiaokong Liu, Liang Li, Panče Naumov, and Hongyu Zhang. Bioinspired soft robots based on organic polymer-crystal hybrid materials with response to temperature and humidity. *Nature Communications*, 14(1), April 2023.

[13] Zhiyuan Zhang, Xueqian Wang, Songtao Wang, Deshan Meng, and Bin Liang. Design and modeling of a parallel-pipe-crawling pneumatic soft robot. *IEEE Access*, 7:134301–134317, 2019.